The effects of mixing on the evolution of intermediate-mass stars of different metallicities

Isabel Renedo

PhD supervisors: Enrique García–Berro & Pilar Gil–Pons

Departament de Física Aplicada, Escola Politécnica Superior de Castelldefels, Universitat Politècnica de Catalunya, Avda. del Canal Olímpic s/n, 08860 Castelldefels, Spain

Abstract

We study the evolution of solar ($Z = 0.016$) and metal-poor stars ($Z = 0.001$) of initial masses corresponding to $2\,M_{\odot}$, and $4M_{\odot}$, from the main sequence until the formation of degenerate carbon-oxygen cores. We explore the nucleosynthesis during the core hydrogen burning phase through the CNO cycle and during the core helium burning phase through the 3α reaction. We determine the combined effects of the nucleosynthesis and of the convective mixing episodes on the surface composition of the considered stars. This work is intended to be a starting point to analyze the effects of more sophisticated treatments of mixing by convection, making special emphasis in the case of metal-poor stars.

1 Introduction

Recent observational surveys are providing us with excellent photometric and high-resolution spectroscopic data. This allows to derive the surface compositions of stars far beyond the solar neighborhood. For instance, the HK survey and the Hamburg/ESO survey have yielded a vast amount of data of stars of the Galactic halo (Christlieb & Beers 2000). Such stars are very old and metal-poor, and their surface composition has posed some challenges to the theory of stellar evolution, as they show amounts of carbon and nitrogen that are significantly different of those of solar-metallicity stars. This abundance pattern is difficult to reconcile with the present theoretical models. In fact, trying to interpret the surface composition of these stars as the result of particular nucleosynthetic and mixing processes during their evolution has become a hot topic in the recent years.

The evolution of intermediate-mass stars involves core hydrogen burning through the CNO cycle, and is followed by the development of hydrogen burning in a shell that surrounds the recently formed helium core. The formation of the hydrogen-burning shell is accompanied by a dramatic increase in the surface radius and luminosity, as well as a decrease in its effective temperature. This important phase in the evolution of stars is known as the Red Giant Branch, and involves not only structural variations, but also changes in the surface composition. The reason is that, as the stellar surface radius increases, the associated layers cool down and a significant temperature gradient develops in the envelope. This leads to the formation of a convective envelope, that begins at the surface but is able to penetrate into layers of the star that have been nuclearly processed. Thus, convection mixes material of the helium core with material of the envelope, whose composition before the mixing practically corresponds to the original composition of the star. Ultimately, the surface abundances of red giant stars reflect both the effects of nucleosynthesis through the CNO cycle and the effects of convective mixing. This mixing process triggered by convection during hydrogen-shell burning is known as the first dredge-up, and it finishes when central helium burning ensues. In fact, as the envelope expands to giant dimensions, the helium core keeps contracting due to its own gravity. Contraction and heating allows the innermost parts of the star to reach the conditions necessary for the ignition of helium through the 3α reactions. These reactions and the $^{12}\mathrm{C}(\alpha,\gamma)^{16}\mathrm{O}$ reaction, that plays an important role at the end of the core helium burning phase, determine the final composition of the degenerate carbon-oxygen core. Furthermore, core helium burning is followed by helium burning in a shell, by a second ascent to the red giant branch, and then by the formation of a deep convective envelope. In this case, convection can mix the material processed by helium and hydrogen burning with the material of the hydrogen-rich envelope that had been previously polluted during the first dredge-up. This second mixing episode is known as the second dredge-up. However, this picture dramatically changes for metal-poor stars and the details of the evolution of this kind of stars are not yet well understood.

This work is an exploratory study of the evolution of moderately metal-poor stars. We will compare our results with those obtained for stars of solar composition of analogous masses. We plan to to extend our calculations to a wider range of masses and metallici-

Table 1: Relevant times and masses at the points labelled as A, B, C and D in Fig. 1. The total masses ($M_{\rm ZAMS}$), the masses of the cores ($M_{\rm core}$) and the mass points corresponding to the base of the convective envelopes ($M_{\rm BCE}$) are expressed in solar units.

Model		A		B			C		D		
$M_{\rm ZAMS}$	Z	$t\,(\times10^{14})$ s	$M_{\rm core}$	$t\,(\times10^{14})$ s	$M_{\rm core}$	$M_{\rm BCE}$	$t\,(\times10^{14})$ s	$M_{\rm core}$	$t(\times10^{14})$ s	$M_{\rm core}$	$M_{\rm BCE}$
4	0.001	175.89	0.729	196.72	1.035	0.983	248.36	0.432	249.69	0.584	0.654
	0.016	283.71	0.713	293.65	0.727	0.658	300.28	0.601	302.07	0.633	0.682
2	0.001	37.11	0.386	37.17	0.432	0.404	47.30	0.405	47.63	0.623	0.622
	0.016	47.40	0.293	51.20	0.652	0.840	66.41	0.390	67.01	0.627	0.627

ties in a near futre and to use more sophisticated treatments of convection and mixing. The present work is organized as follows. In section 2 we briefly describe the physics of our evolutionary code, while in section 3 we analyze the evolution during the hydrogen burning phase and the effects of the first dredge-up. Section 4 is devoted to study the helium burning phase and the second dredge-up. Finally, in section 5 we summarize our results, we draw the main conclusions and we propose future perspectives.

2 Computational details

We use an Eulerian, one-dimensional, hydrostatic code. The nuclear reaction rates are those of Fowler & Caughlan (1988). The code has been updated to include time-dependent mixing (Iben & MacDonald 1985), an extended nuclear network that includes 32 isotopes and allows to compute the carbon-burning phase (García–Berro & Iben 1994), and the new opacity treatment of Iglesias & Rogers (1993), as well as the interpolation of molecular opacities of Ferguson et al. (2005). With these updates (Gil–Pons et al. 2003; 2007), the calculation of the evolution of low- and intermediate-mass stars from the main sequence until late evolutionary stages is feasible for any metallicity range, including both primordial and super-solar compositions. In our calculations convection is treated according to the Schwarzschild criterion, and mixing is instantaneous. This approximation is valid during most of the life of the stars, as the nuclear time scales that determine the evolution are much larger than the time scales associated to mixing by convection. For this work we will use the version of the code that includes a limited nuclear network (9 isotopes from ^{1}H to ^{25}Mg), as it is sufficient to study the first and second dredge-up in our 2 and 4 $M_\odot$ model stars.

3 Hydrogen burning and the first dredge-up

Figure 1 shows the evolution of our model stars in the Hertzsprung-Russell diagram. The evolutionary stages that take place in the lower left regions of this diagram correspond to phases of the evolution in

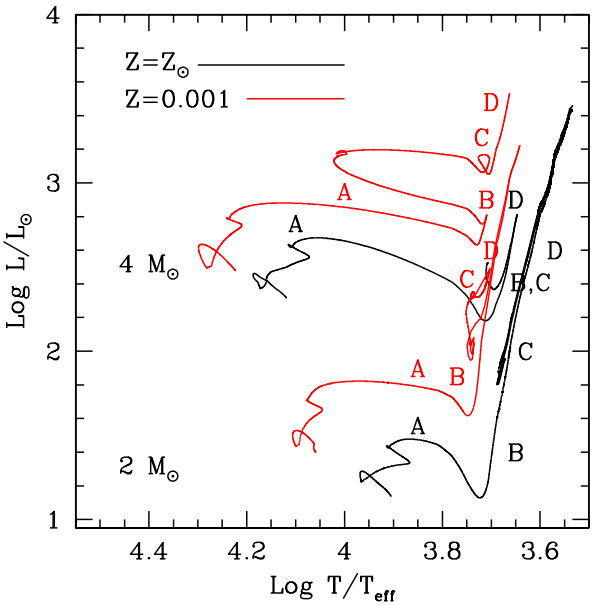

Figure 1: Evolution of the 2 $M_\odot$ and the 4 $M_\odot$ model stars in the Hertzprung-Russell diagram for both the solar-metallicity and metal-poor evolutionary sequences.

which the stars have a relatively compact configuration — their surface temperature is relatively high and their luminosity (and radius) relatively small. On the contrary, the evolutionary stages that occur in the upper right regions of the diagram correspond to phases in which the stars have giant configurations (low surface temperatures and large luminosities and radii). We have labelled the following relevant points in the Hertzsprung-Russell diagram and use this classification through out the rest of this work. The point labelled as "A" is the time at which hydrogen is exhausted at the center of the star. Point "B" is the time at which the base of the convective envelope reaches its innermost mass point during the first ascent of the red giant branch, that is, the first dredge-up. Point "C" corresponds to the time at which helium is exhausted at the center. Finally, the point labelled as "D" is the time at which the base of the convective envelope reaches its innermost mass point during the second ascent of the red giant branch, namely the second drege-up. Note that, in general, metal-poor models are brighter and hotter.

Table 2: Surface abundances of carbon (C), nitrogen (N), and oxygen (O), at the times labelled as A, B (or C, as composition is the same in both cases), and D.

Model		A			B,C			D		
$M_{\rm ZAMS}$	Z	C	N	O	C	N	O	C	N	O
2	0.001	$1.7 \cdot 10^{-4}$	$5.3 \cdot 10^{-5}$	$4.8 \cdot 10^{-4}$	$1.0 \cdot 10^{-4}$	$1.3 \cdot 10^{-4}$	$4.7 \cdot 10^{-4}$	$9.2 \cdot 10^{-5}$	$1.5 \cdot 10^{-4}$	$4.7 \cdot 10^{-4}$
	0.016	$3.4 \cdot 10^{-3}$	$1.1 \cdot 10^{-3}$	$9.6 \cdot 10^{-3}$	$2.8 \cdot 10^{-3}$	$2.3 \cdot 10^{-3}$	$9.6 \cdot 10^{-3}$	$4.9 \cdot 10^{-3}$	$2.3 \cdot 10^{-3}$	$9.1 \cdot 10^{-3}$
4	0.001	$1.7 \cdot 10^{-4}$	$5.3 \cdot 10^{-5}$	$4.8 \cdot 10^{-4}$	$1.5 \cdot 10^{-4}$	$7.3 \cdot 10^{-4}$	$4.8 \cdot 10^{-4}$	$1.0 \cdot 10^{-4}$	$1.3 \cdot 10^{-4}$	$4.8 \cdot 10^{-4}$
	0.016	$3.4 \cdot 10^{-3}$	$1.1 \cdot 10^{-3}$	$9.6 \cdot 10^{-3}$	$2.2 \cdot 10^{-3}$	$2.9 \cdot 10^{-3}$	$9.2 \cdot 10^{-3}$	$2.2 \cdot 10^{-3}$	$3.0 \cdot 10^{-3}$	$9.1 \cdot 10^{-3}$

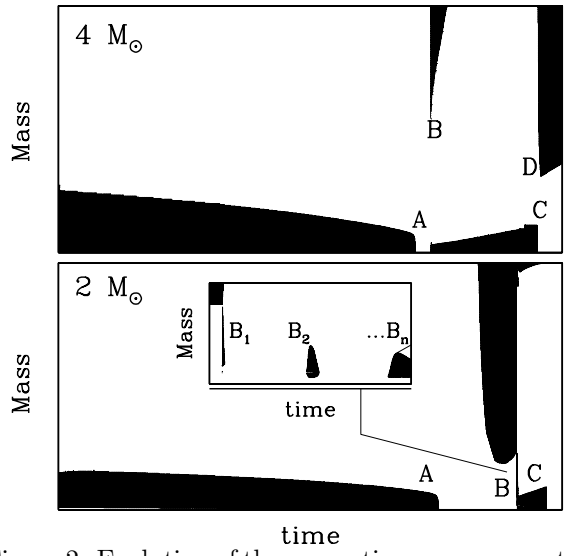

Figure 2: Evolution of the convective zones versus time for the $2\,M_\odot$ and the $4\,M_\odot$ model stars for the metal-poor evolutionary sequences.

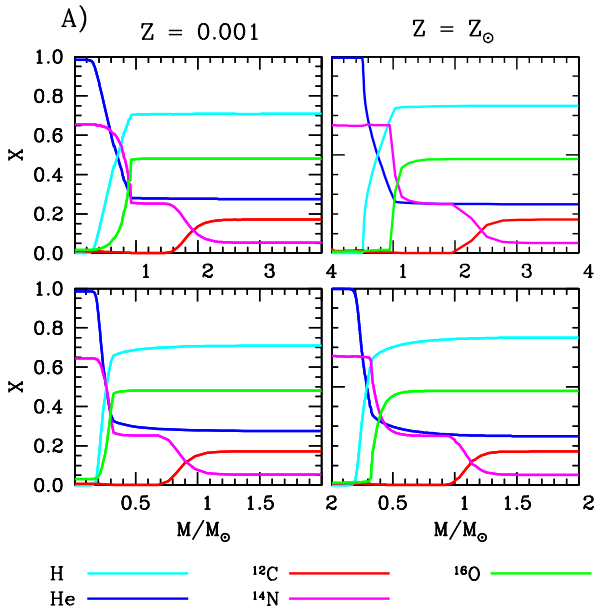

Figure 3: Composition profile of the 2 (bottom panel) and 4 $M_\odot$ (top panel) model stars when hydrogen is exhausted in the core.

Figure 2 shows the Kippenhahn diagram, that is, the evolution of the convective regions of the $4\,M_\odot$ star as a function of time — top panel — and the $2\,M_\odot$ model — bottom panel — from the beginning of the main sequence until the second dredge-up, for both solar composition. We have not labelled the time and mass axis because, even though the qualitative evolution of both stars is the same, the particular values for the times and masses at which the important stages of the evolution occur are different for different metallicities. The points labelled as "A", "B", "C" and "D" correspond to the equivalent points in the Hertzsprung-Russell diagram of Fig. 1 and the corresponding times and masses at these evolutionary stages are shown in Table 1. Core hydrogen burning takes place at relatively large temperatures and low luminosities (up to the point labelled as "A" in Fig. 1). The associated nuclear energy release produces a radiative gradient larger than the adiabatic one in the central regions of the star and, therefore, convection sets in at the center — see shaded areas in Fig. 2. It is worth emphasizing that the density of the cores of the $2\,M_\odot$ models is such that helium burning begins in conditions of partial degeneracy. Therefore, core helium burning does not occur as a single central convective zone but, instead, takes place through a series of off-center flashes that produce small convective regions — see the insert in the lower panel of Fig. 2.

Figure 3 shows the composition profile of our model stars at the end of core hydrogen burning (point "A" in Fig. 1). The upper panels correspond to the $4\,M_\odot$ star whereas the bottom panels correspond to the $2\,M_\odot$ star. For both model stars, the case in which a metal-poor composition has been adopted are shown in the left panels, while the right panels show the profiles when the solar composition is adopted. Note that the abundances of carbon, nitrogen and oxygen have been multiplied by a factor (50 in the case of solar metallicity stars and 10^3 in the case of metal-poor stars) that makes more convenient their visualization. As can be seen, the outermost parts of our model stars in Fig. 3 show the composition of the stellar envelope before any nucleosynthesis or significant mixing process have occured. Therefore, they reflect the initial composition of the star. The innermost parts of the star show the effects of core hydrogen burning through the CNO cycle. Naturally, the core is basically made of helium, but changes have also occured in the less abundant nuclear isotopes. In particular, carbon and oxygen have been depleted and the abun-

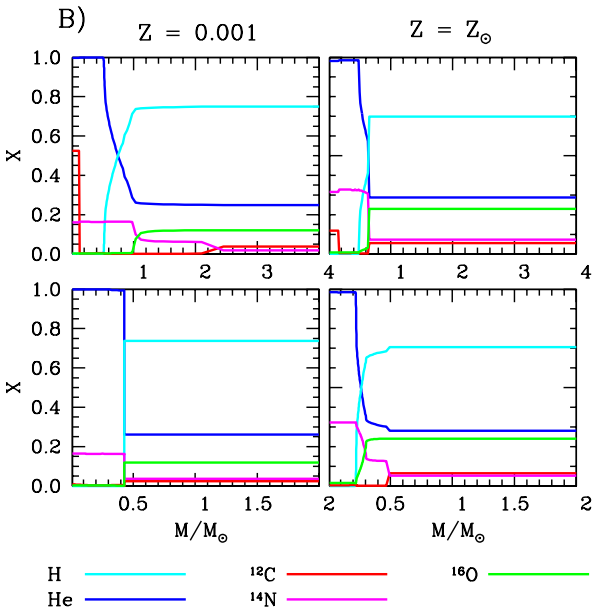

Figure 4: Same as Fig. 3 when the convective envelope reaches its maximum extent inward during the first dredge–up episode.

dance of nitrogen has been enhanced as a consequence of nuclear burning.

When core hydrogen burning finishes and hydrogen burning sets in a shell the surfaces of our model stars cool down and reach giant dimensions. At this time a convective envelope forms and, as explained in the introductory section, mixes matter processed by the CNO cycle with the hydrogen-rich envelope. Figure 4 shows the composition profile of our model stars when the base of the convective envelope reaches its maximum extent inwards (points labelled as "B" in Fig. 1). A flat profile of abundances indicates the presence of a convective region, while the steps in the composition profiles help in locating the edges of the convective regions. A comparison between the abundances shown in figures 3 and 4 reveals the effects of the first dredge-up. In particular, the products of the CNO cycle are mixed in the convective envelope and, therefore, the surface carbon, nitrogen and oxygen abundances shown in Fig. 4 noticeably differ from those of Fig. 3. Additionally, the innermost regions of the metal-poor $2\,M_\odot$ model star in Fig. 4 also show the early effects of helium-burning through the 3α reaction, which produces an increase of the central carbon abundance.

Table 1 shows the values of the core mass ($M_{\rm core}$) — which, in this case is the mass of the hydrogen-exhausted core — and the mass coordinate of the base of the convective envelope ($M_{\rm BCE}$) of selected evolutionary stages, corresponding to the points "A", "B", "C" and "D" described above. When a value of $M_{\rm BCE}$ is smaller than that of the core mass ($M_{\rm core}$ freshly synthesized material is dredged-up from the core to the stellar surface. This occurs for the models which are at the point labelled as "B" in Fig. 1, whose composition is shown in Fig. 4.

4 Helium burning and the second dredge-up episode

The core helium burning phase occurs initially through the 3α reaction. The main effects of the 3α reaction are, from the structural point of view, the end of the core contraction, and the formation of an inner convective core in the $4\,M_\odot$ stellar sequences. Figure 2 shows the convective core during core helium burning as a shaded area between a time occuring shortly after point "B" and point "C". From the point of view of the changes of composition, helium is transformed into carbon and oxygen. In fact core helium does not only burn through the 3α reactions but, instead, when the central helium mass abundance is about 0.2, the reaction $^{12}{\rm C}(\alpha,\gamma)^{16}{\rm O}$ sets in and transforms part of the central carbon into oxygen. Therefore, the stellar core after helium burning is mainly composed of carbon and oxygen.

The $2\,M_\odot$ evolutionary sequences also develop core helium burning. But in these cases their cores have initially smaller temperatures than those of the $4\,M_\odot$ cases and, therefore, helium ignition occurs at much larger pressures (and densities). At these densities the material is partially degenerate and neutrinos efficiently cool the central regions of the star. Thus, helium ignition occurs off-center and helium burning takes place in a series thermonuclear flashes. In these thermonuclear runaways nuclear reactions release significant amounts of energy in short time scales. Consequently, the regions nearby to mass shell where ignition occurs increase their temperature and expand, lifting degeneracy. However, the relevant time scales are such that the nuclear time scale in these regions is shorter than the expansion time scale. Hence, helium is exhausted in these regions and once this occurs the thermonuclear runaway is extinguished. Then the core contracts again and, again, the conditions for helium burning are reached at adjacent regions where a significant helium content alreadys exists. The insert in the lower panel of Figure 2 shows the convective regions that accompany each helium flash. After some flashes occur helium burning reaches the center and the remaining helium is burned in an almost stationary way.

At the end of the helium burning phase, the composition profiles of the resulting $2\,M_\odot$ model stars are similar to those of the $4\,M_\odot$ evolutionary sequences. A carbon-oxygen core is surrounded by a thin carbon-rich layer, and then by a helium-rich and a hydrogen-rich envelope. This can be clearly seen in Fig. 5, where we display the composition profile at time "C" for the 2 and $4\,M_\odot$ model stars. As can be appreciated the thickness of the helium layer is larger for the more

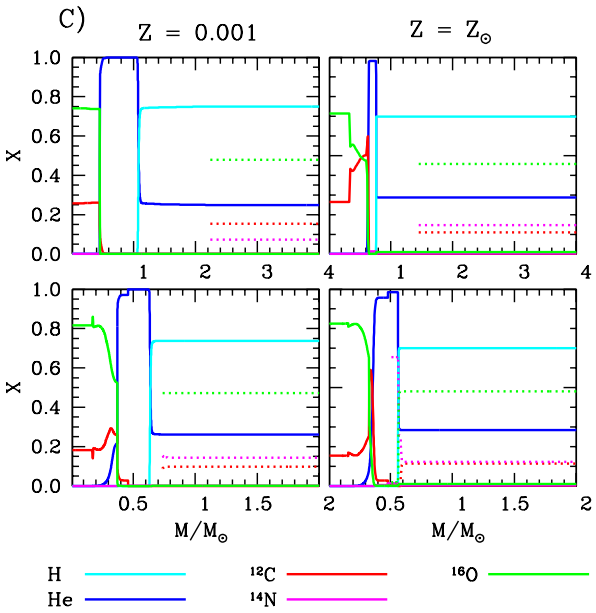

Figure 5: Same as Fig. 3 when helium has been exhausted at the core, and significant helium burning has occured.

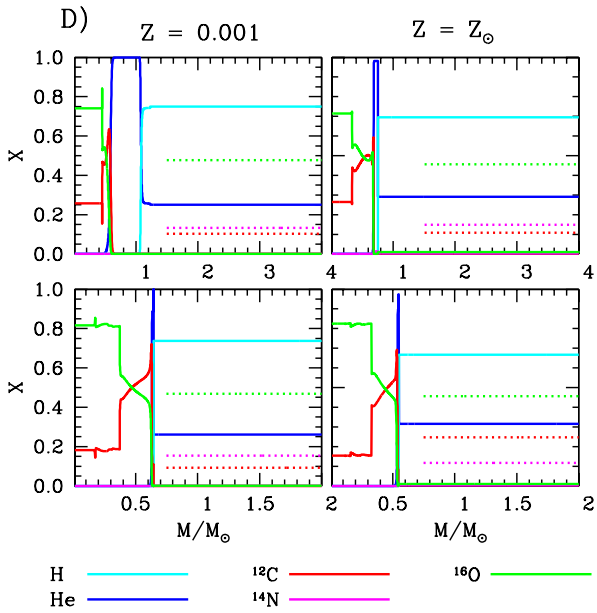

Figure 6: Same as Fig. 3 when the convective envelope reaches its maximum extent inwards during the second dredge-up episode.

metal-poor sequences. It is also worth noting that the convective evelope contains significant amounts of helium. In this case we have represented the envelope abundances of carbon, nitrogen and oxygen, as dotted lines, and again these have been multiplied by a convenient factor for the ease of visualization. These abundances are the same shown in Fig. 4 — corresponding to point "B" — as the stellar envelope does not experience any mixing episode with the core material during the core helium burning phase.

Figure 6 represents the same profiles shown in Fig. 5, but for the times labeled as "D", that is, after the second dredge-up has occured. As can be seen, the helium-rich layers surrounding the core have been practically engulfed in the $2\,M_\odot$ evolutionary sequences, but remain relatively thick for the $4\,M_\odot$ model stars. In none of the cases the stellar envelope has penetrated into the respective carbon-oxygen core. Therefore the effects of the second dredge-up are an increase of the helium and nitrogen abundances, and a decrease of the carbon and oxygen abundances, as it occured during the first dredge-up. In fact, for the $2\,M_\odot$ model sequences, the second dredge-up barely mixes the helium-rich region with the hydrogen-rich envelope. The precise values of the envelope compositions of our model stars are quoted in Table 2 for all the evolutionary stages shown in Figs. 3 to 6.

5 Conclusions and future work

We have followed the evolution of model stars of solar and metal-poor composition of $2\,M_\odot$ and $4\,M_\odot$, paying special attention to the evolution of the central and surface chemical composition. We have analyzed the composition ensuing from core hydrogen burning through the CNO cycle and helium burning through the 3α and the $^{12}\mathrm{C}(\alpha,\gamma)^{16}\mathrm{O}$ reactions, as well as the effects on the surface chemical composition of the first and second dredge-up episodes. Our calculations show that the effects of both dredge-up processes are the mixing of elements processed resulting from hydrogen burning with the material of the envelope. Even though the evolution during core helium burning of the $2\,M_\odot$ models and that of the $4\,M_\odot$ models are very different, the resulting carbon-oxygen cores are qualitatively similar. The subsequent dredge-up processes are not able to mix material synthesized by helium burning with the stellar envelope. Therefore, its effects are merely a second mixing episode of CNO-processed elements.

This work will be extended by computing more advanced stages of the evolution for a grid of models of different masses and metallicities. This includes the so-called thermally-pulsing asymptotic giant branch phase, which is responsible of interesting nucleosynthetic and mixing processes that are extraordinarily sensitive to the computational details. Among these, we mention the treatment of mixing and convection and the spatial and time resolution of the sequences. Our work-plan also includes taking into account thermal diffusion and different treatments of the boundaries of the convective zones and, in particular, diffusive overshooting.

References

Christlieb, N., & Beers, T.C., 2000, in *"Proceedings of the Workshop on Subaru HDS"*, Ed. Takada-Hidai

Ferguson, J.W., Alexander, D.R., Allard, F., Barman, T., Bodnarik, J.G., Hauschildt, P.H., Heffner-Wong, A., & Tamanai, A., 2005, ApJ, **623**, 585

Fowler, W.A., Caughlan, G.R., & Zimmermann, B.A., 1975, ARA&A, **13**, 69

García–Berro, E., & Iben, I., 1994, ApJ, **434**, 306

Gil–Pons, P., Gutiérrez, J., & García–Berro, E., 2007, A&A, **464**, 667

Gil–Pons, P., & García–Berro, E., 2003, A&A, **407**, 1021

Iben, I., Jr., & MacDonald, J., 1985, ApJ **296**, 540

Iglesias, C.A., & Rogers, F.J., 1993, ApJ, **412**, 752